# SYNTHESIS AND GROWTH OF BISMUTH FERRITE ($BiFeO_3$) WITH LANTHANUM (La) AND YTTRIUM(Y) DOPED NANO-STRUCTURES ON ANODIC ALUMINUM OXIDE (AAO) TEMPLATE

A. UR. REHMAN[a], M. W. ASHRAF[a*], S. TAYYABA[b], M. BASHIR[c]
M. F. WASIM[a], M. IMRAN[a],
[a]*Department of Physics (Electronics), GC University Lahore, Pakistan*
[b]*Department of Computer Engineering, the University of Lahore, Pakistan*
[c]*Department of Physics, the University of Punjab, Lahore, Pakistan*

$BiFeO_3$ nanostructures (BFO) have gained enormous consideration owning to the novel size-dependent properties and outstanding multi-ferroic properties at room temperature. In the past few years, research has been carried out to study and characterize BFO and doped BFO structures on various substrates. In this work BFO, Lanthanum doped BFO, Yttrium doped BFO are fabricated on AAO template. The resultant films show the successful in-corporation of BFO, La BFO and Y BFO in nano-porous AAO template. The particle size as well as band-gap shows a decrease due to the addition of BFO, La BFO and Y BFO in nano-porous AAO template.

(Received December 1, 2020; Accepted February 17, 2021)

*Keywords:* Anodic aluminum oxide, Bismuth ferrite, Lanthanum, Yttrium

## 1. Introduction

During the last few decades, vast research has been carried out in the field of multi-ferroic materials. The research mainly comprises of suitable doping of rare earth materials or developing a solid state solution with other perovskite type oxides that changes the multi-ferroic properties of BFO [1-5]. Recently, researchers conduct multiple effort and attempts for the enhancement of properties of Bismuth ferrite (BFO) by addition of rare earth elements like $La^{3+}$,$Pr^{4+}$,$Sm^{3+}$,$Gd^{3+}$ and $Nd^{3+}$ [6-9] as a dopant. This doping of rare earth elements yields a magnetization by dominating the spiral spin structures of BFO. In order to tailor the magneto-electric properties of BFO Co-doping technique is used. Research work has been carried out on the improvement of BFO electrical, optical and ferroelectric properties by using different approaches of doping techniques [9-13]. For improving the magnet moment and local ferromagnetic/ferrimagnetic structure in bismuth ferrite (BFO) Cheng et al. proposed doping of a transition metal of $Bi_{0.8}La_{0.2}Nb_{0.01}Fe_{0.94}TR_{0.05}O_3$ [14]. Recently, considerable attention has been paid to evaluate the influence of pressure, synthesis temperature, annealing and chemical composition on the physical properties and crystal structures of BFO based Nano-powders [15-22]. An easy way to improve the optical and ferroelectric properties of BFO based materials is by doping it with rare earth ion. The outcomes of doping BFO with rare earth ion include decreases in optical band gap and as increase in dielectric constant which is considered an advantage for the formation of functional materials application in multiple devices [23-27].In order to prepare doped BFO nanoparticles molten-salt, co-precipitation, hydrothermal, sol-gel and thermal decomposition techniques have been widely used [28-33]. Due to fast kinetics of reaction, homogenous powder with very fine particles and low initialization temperature, the solution combustion methods have been widely used for the development of BFO nano-particles [34-36]. Lee et al. investigated the influence on multi-ferroic properties and crystal structures of $BiFeO_3$ (BFO) thin film by La doping. Due to the enriched crystallinity and increase in lattice parameters of La doped BFO films; the increase is seen in the remnant polarization and dielectric constant of the prepared film. Similarly, the fatigue behavior of $BiFeO_3$ (BFO) and polarization switching was significantly increased. At room temperature, the

* Corresponding author: muhammad.waseem.ashraf@gmail.com

BFO films magnetization increased with the increase in La doping. Wang et al. used Polycarbonate (PC) membrane template-assisted electro-deposition method for the preparation of Y-Fe alloy nanowires from the aqueous solution of Citric acid as a complexing agent. The result revealed that there was a shift in the nanowires structures from semi-crystalline to amorphous due to the change in Y-content. Suharno et al. used sol-gel method for the synthesis of Pure and Y-doped $BiFeO_3$ to study the dielectric and structural properties. The results revealed that Y-doped $BiFeO_3$ indicates the reduction of the rhombohedra phase and increased the orthorhombic phase. The particle size was reduced to 200-400 nm due to doping of Yttrium. The value of impedance of $BiFeO_3$ and Y doped decreases at low frequency (40 – 2 kHz) but after a frequency of 2 kHz it has a constant value. The pure and Y-doped $BiFeO_3$ have a constant dielectric constant after frequency 2 kHz and decreasing at low frequency (40 – 2 kHz).Similarly, the conductance of pure $BiFeO_3$ is smaller than Y-doped $BiFeO_3$ at 42 Hz – 5 MHz and after 2 kHz frequency conductance of Y doped increases significantly. Hossain et al. studied the advantages of La doping in $BiFeO_3$ (BFO) by using a hydrothermal method with an average size of nanoparticles is 50-60nm. At room temperature, the nonlinear M-H loops accompanied improve magnetic moment and large coercivity. By La doping, the low leakage current is achieved [37]. Adhlakha et al. used sol-gel method for the preparation of Polycrystalline phase pure $BiFeO_3$ (BFO) and co-doped $Bi_{0.95}La_{0.05}Fe_{1-x}Y_xO_3$ (with x=0.05, 0.10, 0.15 and 0.20) ceramics. The result shows that Y and La co-doped ceramics shows structural transition. These transitions are from rhombohedral to orthorhombic phase for $x \geq 0.10$ of yttrium doping concentration. An increase in co-doping of Y content in $BiFeO_3$ considerably improve the magnetization, magneto capacitance and dielectric constant and result in a decrease in band gap and average grain size [38].

It has been observed that the substitution of lanthanide elements (La, Nd, Sm) at Bi site and $La^{3+}$ doping at A site of BFO is effective in decreasing the leakage current density furthermore increasing the electrical and magnetic properties [39-40]. However, the addition of $La^{3+}$ ion at Bi site not ensure the distortion in the lattice due to the similarity of ionic radius $La^{3+}$ (1.16 Å) and $Bi^{3+}$ (1.15 Å) [41]. The rhombohedral structures of $BiFeO_3$ are maintained due to the substitution of $Bi^{3+}$ by 5 mol% $La^{3+}$ at A site and its accumulation stabilizes the perovskite phase and increases the ferromagnetic properties [42].The solid solution of $YFeO_3$ with $BiFeO_3$ also made it possible for the improvement of multi-ferroic properties [43]. Palkar et al. substituted La at A site and Mn at B site in $BiFeO_3$ to study the enhancement effect of the magnetic properties[44].Liu et al reported that the doping of Ce/Zr with $BiFeO_3$ thin film reduced the dielectric loss and leakage current density[45].Many researcher co-substitute A-site of ($Bi^{3+}$) with $La^{3+}$ and B-site with $Nb^{5+}$,$Zr^{4+}$ and $Ti^{4+}$ions concurrently in $BiFeO_3$.These substitutions are effective in reducing the leakage current and enhancing the magnetic and electrical properties[46-47]. The co-doping of $La^{3+}$ and $Y^{3+}$ with $BiFeO_3$ displays attractive optical properties due to its small band gap and also makes it a promising candidate for photoconductivity and photo-catalysis. However, there are a few reports on the optical properties of $BiFeO_3$ [48-49].

In this paper, the authors investigate the optical and structural properties of BFO, La and Y nano-structures on anodic aluminum oxide template. Anodization method is opted to synthesize AAO template. The AAO template was used as a substrate for the growth of La, Y and BFO nanostructures.

## 2. Methodology

### 2.1. Synthesis of AAO templates

Aluminum sheet having size 20×20 mm and thickness 0.25 mm was used as a template for the anodization by well-known two-step Anodization [50-51]. The average nano-pores size of the electrochemically fabricated AAO template is approximately equals to 85 nm. First, the aluminum sheet was ultrasonically cleaned in acetone and de-ionized water for 10 minutes each to remove all impurities. Aluminum sheet was furthermore electro-polished using voltage of 30 Volts at temperature 0 $^{O}$C for 10 minutes in ethanol and per-chloric acid respectively. The dissolved chemical solution was magnetically stirred with 1200 revolution per minute. The first step of

anodization was performed for 4 hours using a 0.3M Oxalic acid solution under an isothermal condition at 15$^{o}$C followed by the Galvano-static condition at 15 mA cm$^{-2}$. After the first step of anodization the Anodized AAO-template was etched in 2.0 wt. % chromic acid and 6.0 at wt% phosphoric acid solution at 35$^{o}$C for 25 min. After etching, the second step of anodization was performed for 10 hours with the same conditions as the first step of anodization. The voltage during second step of anodization was kept constant at 40 V at a temperature of 0$^{o}$C respectively. Figure 1 shows the basic AAO template fabrication schematic.

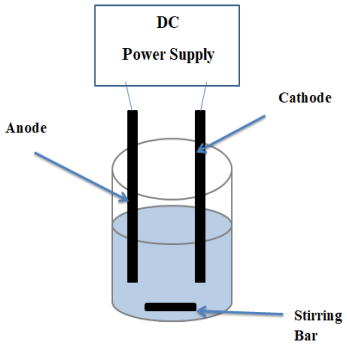


*Fig. 1. Basic fabrication setup for AAO template.*

### 2.2. Growth of BFO and Y-BFO nano-structures on AAO-Template

In order to grow the nanostructures of BFO on AAO template, Fe $(NO_3)_3{\cdot}9H_2O$, Bi $(NO_3)_2{\cdot}5H_2O$ and $NH_4F$ are mixed in a ratio of 1.5:3.5 in ethanol and deionized water. The solution was stirred for 15 minutes and then transferred to 40 ml Teflon cavity. For the growth of BFO nano-structures, the fabricated AAO template was immersed in this solution and was thermally treated at 100°C for 5 hours. AAO-template with BFO nanostructures was washed thrice in ethanol solution. After washing this template was again transferred into the muffle furnace at 300°C for 4 h.

For the growth of yttrium nano-structures on AAO template with BFO nanostructures, 5% of yttrium Oxide ($Y_2O_3$) was first dissolved in deionized water and homogenous acetic acid solution is added drop-wise. For the growth of nanostructures of Yttrium substitutes BFO nanostructures on AAO-template the homogenous acetic acid solution was stirred at 80 °C. Then by drop-wise addition on AAO-template the Yttrium substitutes BFO nanostructures were grown.

### 2.3. Growth of BFO and La-BFO nano-structures on AAO-Template

An auto-combustion sol–gel technique is used to synthesize the $BiFeO_3$ with $La_{0.1}Bi_{0.9}FeO_3$ nanoparticles containing 5% of La content. The raw hydrated nitrate chemicals including $4BiNO_3(OH)_2{\cdot}BiO(OH)$, $La(NO_3)_3{\cdot}6H_2O$ and $Fe(NO_3)_3{\cdot}9H_2O$, were acquired as La, Bi and Fe sources. After the completion of the reaction, the assimilated nanoparticles were thermally annealed at 600 $^{o}$C and decorated on AAO templates. The prepared samples are shown in Table 1.

*Table 1. Prepared samples name and types.*

| Sample Name | Sample type |
|---|---|
| **S1** | AAO template |
| **S2** | BFO nano-structures on AAO template |
| **S3** | Y doped BFO nano-structures on AAO template |
| **S4** | La doped BFO nano-structures on AAO template |

### 2.4. Characterization

The prepared La and Y doped BFO deposited on AAO templates are characterized to study its structural, optical and chemical composition using various characterization techniques. Scanning electron microscopy was used to analyze the structure and morphology of the prepared thin films. Ultra-violet spectrophotometer was used to study the optical behavior of the prepared film. X-ray diffraction method was used to study the chemical composition of the prepared BFO doped structures on AAO template.

## 3. Results and discussion

### 3.1. Structural and chemical analysis

The structural analysis of the prepared samples was performed using X-ray diffraction with $2\theta$ scanning range of 10°-80°. Fig. 2 shows the x-ray diffraction result of the nano-porous AAO membrane, BFO on nano-porous AAO membrane, La doped BFO on AAO and Y doped BFO on AAO. Fig. 2 (a) shows the diffraction peaks of $Al_2O_3$ pattern having rhombohedral geometry which are in accordance with the ICDD data set number 00-001-1243. In case of BFO on AAO template as shown in Fig. 2 (b), XRD peaks were broadened with less intense peaks. An additional peak at 50.5° can be seen which is due to the rhombohedral geometry of $BiFeO_3$ structure which depicts the successful growth of BFO on AAO template. In case of Y doped BFO on AAO template, as shown in Fig. 2 (c), an additional peak can be seen at $2\theta$ values of 30.24° which was due to the cubic phase $Y_2O_3$ structure which shows the proper in-capsulation of Y in BFO. In case of La doped BFO as shown in Fig. 2 (d), the XRD diffraction peak is broader and less in intensity as compare to BFO nano-structures. Using the sherrer's formula, the calculated crystallite size decreases with BFO and Y as well as La doped BFO on AAO template. This effect can be attributed to the smaller ionic radii of La as well as Y as compared to Bi. A similar trend has been seen for lattice parameters.

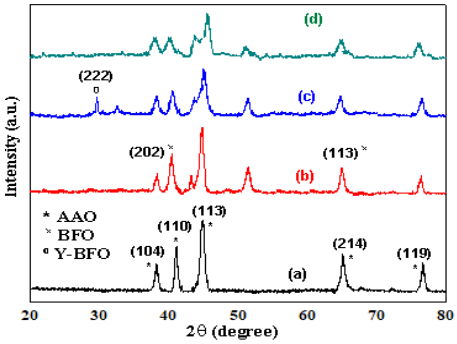


*Fig. 2. X-ray diffraction analysis of (a) nano-porous AAO (b) BFO on AAO (c) Y doped BFO on AAO (d) La doped BFO on AAO.*

### 3.2. Morphological analysis

The structural analysis and morphology of the prepared BFO doped nanostructures on AAO template was studied using scanning electron microscopy.

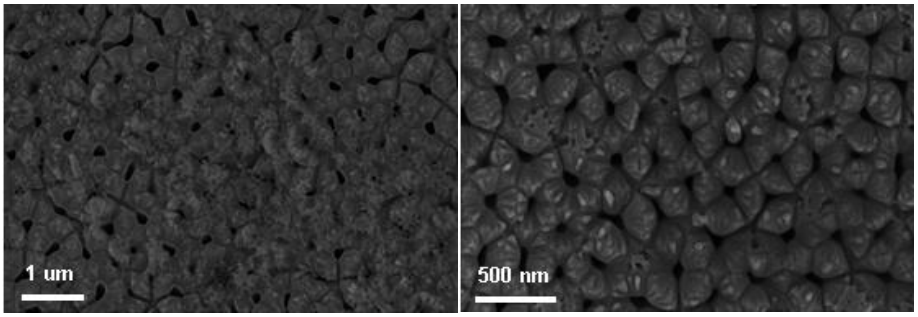


*a)* *b)*

*Fig. 3. SEM image of AAO template with magnification of (a) 1 um (b) 500 nm.*

Fig. 3 shows highly ordered nano-porous AAO membrane. The hexagonal, highly symmetric pores of the prepared AAO template with a pore size of 70-80 nm can be seen in Fig. 3. Fig. 3 (a) shows AAO template with a magnification of 1 um. With a 500 nm magnification as shown in Fig. 3 (b), highly structural nano-porous membrane can be seen.

Fig. 4 (a) shows BFO nano-structures grown on AAO substrate. These films show diamond shaped morphology which is similar to the morphology of BFO nano-structures.

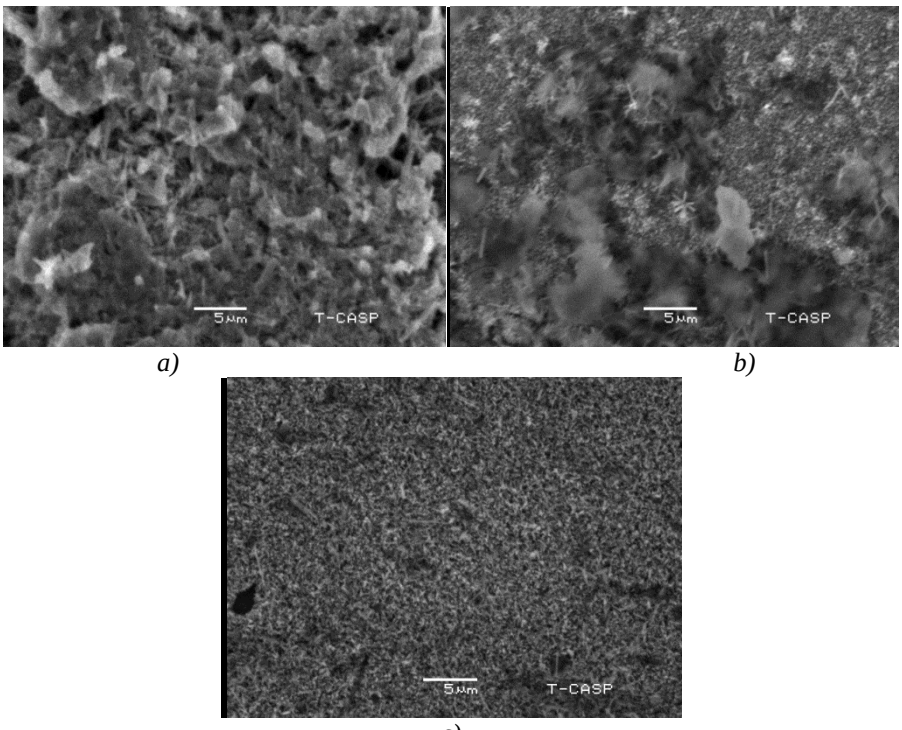


*a)* *b)*

*c)*

*Fig. 4. SEM micrographs of (a) BFO deposited on AAO (b) Y doped BFO deposited on AAO (c) La doped BFO deposited on AAO.*

With La doping as shown in Fig. 4 (b), round shaped La doped BFO nanostructures can be seen on AAO substrate. The size of the prepared La doped BFO nanostructures on AAO is smaller than BFO nanostructures which can be seen in X-ray diffraction analysis. These with Y-doping in BFO nanostructures deposited on AAO template, flakes like structures can be seen on the substrate as shown in Fig. 4 (c). As seen in crystallographic analysis, presence of these flakes can be attributed to the presence of Yttria enriched areas.

### 3.3. Optical analysis

The optical properties of the prepared films were analyzed using UV-Vis spectrophotometer in the wavelength range of 300-1100 nm. Fig. 5 shows the UV-Vis spectrophotometer results of the prepared BFO-AAO and doped BFO AAO substrate. The figure shows a blue shift of absorbance towards left which depicts the decrease in band-gap. By extra plotting the tangents at x-axis the absorbance off-set for the doped and un-doped substrate are calculated. The increase in absorbance off-set can be attributed to the filling of AAO nano-pores. Using the tauc plot the band-gap of the films were calculated based on the absorbance off-set. The calculated absorbance off-set as well as band-gap of the prepared films are shown in Table 2.

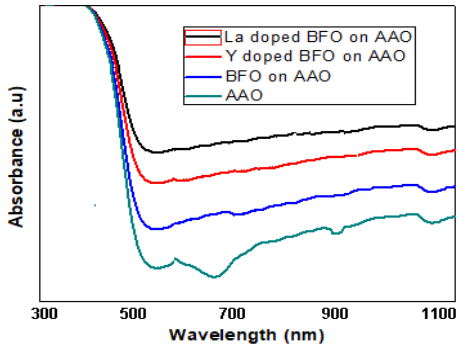


*Fig. 5. UV-vis spectrophotometer results of the prepared AAO, BFO on AAO, Y doped BFO on AAO and La doped BFO on AAO.*

A decrease in optical band-gap can be observed with the addition of La and Y in the BFO AAO substrate. This effect can be due to quantum confinement effect due to the decrease in size of particle of BFO with the addition of La and Y.

*Table 2. Calculated absorbance off-set and band-gap for prepared AAO, BFO on AAO, La doped BFO on AAO and La doped BFO on AAO.*

| Sample Name | Absorbance off-set | Band-gap |
|---|---|---|
| S1 (AAO) | 515 | 2.4 |
| S2 (BFO on AAO) | 532 | 2.33 |
| S3 (Y doped BFO on AAO) | 548 | 2.26 |
| S4 (La doped BFO on AAO) | 557 | 2.23 |

## 4. Conclusion

In this work, synthesis and characterization of AAO templates, thin films of BFO, La doped BFO and Y doped BFO were carried out. Uniform and smooth nano-porous AAO patterned templates were successfully fabricated. Then BFO, La doped BFO and Y doped BFO nanostructures were deposited on the porous template. The results depict the decrease in pore size of AAO template with the deposition of metal doped BFO. The optical band gap was found to decrease considerably from 2.4 eV to 2.26 eV and 2.23 eV due to addition of Y BFO and La BFO nanoparticles, respectively, on nano-porous AAO-templates.

## References

[1] A. Mukherjee, M. Banerjee, S. Basu, P. M. G. Nambissan, M. Pal, J. Phys. D: Appl. Phys. **46**, 495309 (2013).
[2] A. Mukherjee, S. Basu, G. Chakraborty, M. Pal, J. Appl. Phys. **112**, 014321 (2012).

[3] G. L. Yuan, S. W. Or, J. M. Liu, Z. G. Liu, Appl. Phys. Lett. **89**, 052905 (2006).
[4] C.-H. Yang, J. Seidel, S. Y. Kim, P. B. Rossen, P. Yu, M. Gajek, Y. H. Chu, L. W. Martin, M. B. Holcomb, Q. He, P. Maksymovych, N. Balke, S. V. Kalinin, A. P. Baddorf, S. R. Basu, M. L. Scullin, R. Ramesh, Nat. Mater. **8**, 485 (2009).
[5] T. Kanai, S. I. Ohkoshi, A. Nakajima, T Watanabe, K. Hashimoto, Adv. Mater. **13**, 487 (2001).
[6] S. T. Zhang, Y. Zhang, M. H. Lu, C. L. Du, Y. F. Chen, Z. G. Liu, Y. Y. Zhu, N. B. Ming, X. Q. Pan, Appl. Phys. Lett. **88**, (1629012006).
[7] F. Z. Huang, X. M. Lu, W. W. Lin, X. M. Wu, Y. Kan, J. S. Zhu, Appl. Phys. Lett. **89**, 242914 (2006).
[8] V. A. Khomchenko, D. A. Kiselev, I. K. Bdikin, V. V. Shvartsman, P. Borisov, W. Kleemann, J. M. Vieira, A. L. Kholkin, Appl. Phys. Lett. **93**, 262905 (2008).
[9] F. Yu, M. Y. Li, Z. Q. Hu, L. Pei, D. Y. Guo, X. Z. Zhao, S. X. Dong, Appl. Phys. Lett. **93**, 182909 (2008).
[10] G. L Yuan, Or. S. Wing, J. Appl. Phys. **100**, 024109 (2006).
[11] Sk. M. Hossain, A. Mukherjee, S. Chakraborty, S. M. Yusuf, S. Basu, M. Pal, Mater. Focus **2**, 1 (2013).
[12] A. Mukherjee, Sk. M. Hossain, S. Basu, M. Pal, Appl. Nanosci. **2**, 305 (2012).
[13] Sk. M. Hossain, A. Mukherjee, S. Basu, M. Pal, Micro Nano Lett. **8**, 374 (2013).
[14] Z. X. Cheng, X. L. Wang, Y. Du, S. X. Dou, J. Phys. D: Appl. Phys. **43**, 242001 (2010).
[15] B. Ahmmad, K. Kanomata, K. Koike et al., Journal of Physics D: Applied Physics **49**(26), 265003 (2016).
[16] G. S. Arya, N. S. Negi, Journal of Physics D: Applied Physics **46**(9), 095004 (2013).
[17] K. Brinkman, T. Iijima, H. Takamura, Japanese Journal of Applied Physics **46**(4), L9 (2007).
[18] A. ur. Rehman, M. W. Ashraf, A. Mahmood, A. u. Rehman, S. M. Ramay, and M. Saleem, Physica E: Low-dimensional Systems and Nanostructures, **127**, 114513, (2021).
[19] A. ur. Rehman, M. W. Ashraf, S. Tayyaba, S. M. Ali, S. M. Ramay, and M. Saleem, Materials Letters, **244**, 115-118, (2019).
[20] R. Haumont, J. Kreisel, P. Bouvier, Phase Transitions **79**(12), 1043 (2006).
[21] N. A. Lomanov, V. V. Gusarov, Nanosystems: Physics, Chemistry, Mathematics **4**, 696 (2013).
[22] G. F. Cheng, Y. J. Ruan, W. Liu, X. S. Wu, Materials Letters **143**, 330 (2015).
[23] P. Suresh, P. D. Babu, S. Srinath, Ceramics International **42**(3), 4176 (2016).
[24] S. Madolappa, S. Kundu, R. Bhimireddi, K. B. R. Varma, Materials Research Express **3**(6), 2016.
[25] B. Yotburut, T. Yamwong, P. Thongbai, S. Maensiri, Japanese Journal of Applied Physics **53**(6S), 06JG13 (2014).
[26] A. ur-rehman, M. W. Ashraf, H. Shaikh, A. Alhamidi, S. M. Ramay, and M. Saleem, Ceramics International, **46**, 7681-7686, (2020).
[27] R. Das, G. G. Khan, S. Varma, G. D. Mukherjee, K. Mandal, The Journal of Physical Chemistry C **117**(39), 20209 (2013).
[28] G. Dhir, P. Uniyal, N. K. Verma, Journal of Magnetism and Magnetic Materials **394**, 372 (2015).
[29] J. Wang, Y. Wei, J. Zhang, L. Ji, Y. Huang, Z. Chen, Materials Letters **124**, 242 (2014).
[30] M. Y. Shami, M. S. Awan, M. Anis-ur-Rehman, Journal of Alloys and Compounds **509**(41), 10139 (2011).
[31] J.-H. Xu, H. Ke, D.-C. Jia, W. Wang, Y. Zhou, Journal of Alloys and Compounds **472**(1-2), 473 (2009).
[32] S. Li, G. Zhang, H. Zheng, N. Wang, Y. Zheng, P. Wang, RSC Advances **6**(85), 82439 (2016).
[33] S. M. Selbach, M.-A. Einarsrud, T. Tybell, T. Grande, Journal of the American Ceramic Society **90**(11), 3430 (2007).
[34] M. Hasanand, M. F. Islam, International Journal of Advanced Engineering and Nano Technology **2**, 1 (2015).
[35] K. C. Patil, M. S. Hegde, T. Rattan, S. T. Aruna, Chemistry of Nanocrystalline Oxide

Materials. Combustion Synthesis, Properties and Applications, World Scientific Publishing Co. Pte. Ltd, Singapore, 2008.
[36] F. Deganello, G. Marcì, G. Deganello, Journal of the European Ceramic Society **29**(3), 439 (2009).
[37] Z. X. Cheng, A. H. Li, X. L. Wang, S. X. Dou, K. Ozawa, H. Kimura, S. J. Zhang, T. R. Shrout, J. Appl. Phys. **103**, E507 (2008).
[38] G. L. Yuan, S. W. Or, Appl. Phys. Lett. **88**, 062905 (2006).
[39] G. L. Song, H. X. Zhang, T. X. Wang, H. G. Yang, F. G. Chang, J. Magn. Magn. Mater. **324**, 2121 (2012).
[40] K. S. Nalwa, A. Garg, J. Appl. Phys. **103**, 044101 (2008).
[41] H. Singh, K. L. Yadav, J. Phys.: Condens. Matter **23**, 385901 (2011).
[42] R. K. Mishra, D. K. Pradhan, R. N. P. Choudhary, and A. Banerjee, J. Mag. Mag. Mater. **320**, 2602 (2008).
[43] V. R. Palkar, D. C. Kundaliya, S. K. Malik, J. Appl. Phys. **93**, 4337 (2003).
[44] J. Liu, M. Li, L. Pei, J. Wang, Z. Hu, X. Wang, X. Zhao, EPL **89**, 57004 (2010).
[45] C. Lan, Y. Jiang, S. Yang, J. Mater. Sci. **46**, 734 (2011).
[46] Y. F. Cui, Y. G. Zhao, L. B. Luo, J. J. Yang, H. Chang et al., Appl. Phys. Lett. **97**, 222904 (2010).
[47] X. Chen, H. Zhang, T. Wang, F. Wang, W. Shi, Phys. Status Solidi A **209**, 1456 (2012).
[48] P. Chen, N. J. Podraza, X. S. Xu, A. Melville, E. Vlahos, V. Gopalan, R. Ramesh, D. G. Schlom, J. L. Musfeldt, Appl. Phys. Lett. **96**, 131907 (2010).
[49] X. S. Xu, T. V. Brinzari, S. Lee, Y. H. Chu, L. W. Martin, A. Kumar, S. McGill, R. C. Rai, R. Ramesh, V. Gopalan, S. W. Cheong, J. L. Musfeldt, Phys. Rev. B **79**, 134425 (2009).
[50] M. F. Wasim, M. W. Ashraf, S. Tayyaba, A. S. Nazir, Digest Journal of Nanomaterials and Biostructures, **14 (3)**, (2019).
[51] B. ALI, S. TAYYABA, M. W. ASHRAF, M. W. NAWAZ, M. T. MUSHTAQ, M. AKHLAQ, M. F.WASIM, Digest Journal of Nanomaterials and Biostructures, **15 (2)**, (2020).